Nuclear Resonant Scattering on Earth Materials using Synchrotron Radiation

Program/Abstracts Book

February 12-13, 2005
Advanced Photon Source
Argonne National Laboratory
Argonne, IL

COMPRES

Supported by the National Science Foundation

Office of Science
U.S. DEPARTMENT OF ENERGY

THE UNIVERSITY OF CHICAGO

ARGONNE NATIONAL LABORATORY

Argonne is operated by The University of Chicago for the U.S. Department of Energy Office of Science

TABLE OF CONTENTS

Nuclear Resonant Scattering on Earth Materials using Synchrotron Radiation

Program

Nuclear Resonant Scattering 2005

COMPRES

Supported by the
National Science Foundation

Office of Science
U.S. DEPARTMENT OF ENERGY

THE UNIVERSITY OF CHICAGO

ARGONNE NATIONAL LABORATORY

Argonne is operated by The University of Chicago for the U.S. Department of Energy Office of Science

Friday, Feb. 11th

7:00 p.m. **Reception at Argonne Guest House**

Saturday, Feb. 12th

Morning Session, Building 402, Room E-1100
Chair: *Jay D. Bass*

9:00 a.m. **Welcome**
Wolfgang Sturhahn, Advanced Photon Source

9:15 a.m. **Prospective for Nuclear Resonant X-Ray Spectroscopy as a Major Tool for Deep Earth Studies**
Ho-kwang Mao, Carnegie Institution of Washington

10:00 a.m. **An Introduction to Nuclear Resonant Spectroscopy**
Wolfgang Sturhahn, Advanced Photon Source

10:45 a.m. **Coffee Break**

11:15 a.m. **Applications of NRIXS and NFS Techniques at High Pressures**
Viktor V. Struzhkin, Carnegie Institution of Washington

11:50 a.m. **Nuclear Resonant Inelastic X-Ray Scattering and Synchrotron Mössbauer Spectroscopy with Laser-Heated Diamond Anvil Cells**
Jung-Fu Lin, Carnegie Institution of Washington

12:25 p.m. **Lunch**
Gallery of Building 402

Afternoon session, Building 402, Room E 1100
Chair: Ho-kwang Mao

2:00 p.m. **Measuring Velocity of Sound with Nuclear Resonant Inelastic X-Ray Scattering**
Michael Hu, HP-CAT & Carnegie Institution of Washington

2:35 p.m. **Nuclear Resonant X-Ray Scattering of Iron Hydride at High Pressure**
Wendy Mao, The University of Chicago

3:10 p.m. **Nuclear Resonant Inelastic X-Ray Scattering from ^{83}Kr**
Jiyong Zhao, Advanced Photon Source

3:45 p.m. **Coffee Break**

4:15 p.m. **Iron Valence, Lattice Distortion, and Spin Crossover in (Mg,Fe)SiO_3 Perosvkite: A Synchrotron Mössbauer Spectroscopy Study to 120 GPa**
Jennifer M. Jackson, University of Illiniois at Urbana-Champaign

4:50 a.m. **Synchrotron Mössbauer Spectroscopy at High Pressure and High Temperature**
Guoyin Shen, CARS-CAT & University of Chicago

6:30 p.m. **Dinner**
Guesthouse

Sunday, Feb. 13th

9:00 a.m. **Introduction to the Experiments**
Wolfgang Sturhahn, Advanced Photon Source (Building 431, Room C-010)

9:30 a.m. **Experiments at Sector 3**

10:30 a.m. **Coffee Break**
Building 431, Room C-010

11:00 a.m. **Experiments at Sector 3**

12:30 p.m. **Lunch**
Gallery of Building 402

2:00 p.m. **Experiments at Sector 3**

4:00 p.m. **Coffee Break**
Building 431, Room C-010

4:30 p.m. **Experiments at Sector 3**

5:00 p.m. **Near Term Prospects for Nuclear Resonant Scattering at the APS**
Ercan E. Alp, Advanced Photon Source (Building 402, Room E-1100)

Nuclear Resonant Scattering on Earth Materials using Synchrotron Radiation

Abstracts

Nuclear Resonant Scattering 2005

COMPRES

Supported by the
National Science Foundation

Office of Science
U.S. DEPARTMENT OF ENERGY

THE UNIVERSITY OF CHICAGO

ARGONNE NATIONAL LABORATORY

Argonne is operated by The University of Chicago for the U.S. Department of Energy Office of Science

Prospective for Nuclear Resonant X-Ray Spectroscopy as a Major Tool for Deep Earth Studies

Ho-kwang Mao[1] and Wendy Mao[2]
[1]Carnegie Institution of Washington, Washington, D.C.
[2]The University of Chicago, Chicago, IL

After the initial phase of exciting reconnaissance high *P-T* studies, tapping the full potential of nuclear resonant x-ray spectroscopy (NRXS) awaits expanded depth, breadth, and accuracy of the technique as well as the integration of NRXS with other experimental and theoretical approaches.

For pure iron, only the initial slope of the phonon density of state (DOS) at high *P-T* has been used extensively for measurements of aggregate sound velocities which are some of the many key parameters necessary for constraining the properties of the Earth's core. Potentially most of the other parameters can also be derived from NRXS. Accurate determination of the initial slope of strongly textured ε-Fe sample under uniaxial compression can provide elastic anisotropy information when combined with radial x-ray diffraction (XRD) study. Conversely, accurate determination of the initial slope of a polycrystalline ε-Fe sample under hydrostatic *P* can yield single-crystal elastic moduli C_{ij} when combined with hydrostatic XRD and nonhydrostatic non-resonant x-ray inelastic scattering measurements. Moreover, precise determination of van Hove singularities and the detailed shape of DOS can provide the most stringent constraints to elasticity calculations from *ab-initio* theory which is currently the only method capable of reaching the entire *P-T* range of the core. The effects of magnetism and anharmonicity of Fe at high *P-T* also need to be treated theoretically. The integration of the DOS provides heat capacity and entropy information which can be used for resolving the Clapeyron slopes of α–γ–ε phase relations when combined with XRD. Furthermore, the integration of entropy and combination with XRD results can yield the Debye temperature (Θ) and Grüneisen parameter (γ) at high *P-T*.

To extend NRXS applications beyond pure iron, we need to establish the effects of other components to the DOS, by theory and by experiment over a wide range of well characterized materials at ambient conditions. Once fully established, with Fe, Sn, Kr, and Dy which represent a wide range of geochemical properties, NRXS may eventually become a major tool for deep Earth studies.

An Introduction to Nuclear Resonant Spectroscopy

Wolfgang Sturhahn
Advanced Photon Source, Argonne National Laboratory, Argonne, IL

In recent years, nuclear resonant scattering techniques that utilize synchrotron radiation have provided new opportunities for the study of vibrational and magnetic properties of condensed matter under extreme conditions. In particular, the determination of the vibrational density of states with nuclear resonant inelastic x-ray scattering (NRIXS) and the study of valencies and magnetic properties with synchrotron Mössbauer spectroscopy (SMS) provided unique results.

In this contribution, we offer an introduction to nuclear resonant scattering on a basic level and motivate applications in the high-pressure and high-temperature sector relevant to the geophysical problem area. We will individually address NRIXS, a method that uses probe nuclei with suitable resonances to measure the vibrational density of states, and SMS for the determination of valencies and spin states. The response of a nuclear resonance to a synchrotron radiation pulse is delayed in time, a consequence of the narrow resonance-line width. Electronic scattering (the common form of x-ray scattering) happens almost immediately after excitation and therefore can be efficiently discriminated against. For NRIXS, this "time discrimination trick" permits excellent signal-to-noise ratios even for small amounts of resonant material (less than 1ng for iron metal) surrounded by large amounts of non-resonant material. The SMS technique uses the specific pattern of the nuclear time response to evaluate the effect of the electronic environment on the nucleus. Subtle changes in the 3d configuration of Fe are thus detectable. The measured signal is always specific to the nuclear resonant isotope, e.g., ^{57}Fe, ^{83}Kr, ^{119}Sn, and thus the NRIXS and SMS techniques provide the experimenter with perfect isotope selectivity.

Both methods are very sensitive to small amounts of material and take advantage of the high brilliance of synchrotron radiation, which makes micrometer-sized x-ray beams with high intensity possible. These properties together with the isotope selectivity allowed NRIXS and SMS investigations on materials under pressures in the Mbar regime using diamond anvil cells. The introduction of Laser heating in combination with NRIXS and SMS at sector 3-ID of the Advanced Photon Source permits us now to conduct these studies under high pressure and high temperature.

This work is supported by the U.S. DOE-BES, Office of Science, under Contract No. W-31-109-Eng-38.

Applications of NRIXS and NFS Techniques at High Pressures

Viktor V. Struzhkin
Geophysical Laboratory, Carnegie Institution of Washington, Washington, D.C.

Compression of a solid allows to tune interatomic distances and induce a variety of transitions (e. g. insulator-metal transitions, spin-crossover transitions, etc..) in variety of materials. The most widely used technique for this purpose - diamond anvil cell (DAC) technology - has developed rapidly over the past few years. A number of techniques, which were previously limited to ambient and low pressure (because of the requirement of a large sample volume), may now be used at high and even ultrahigh pressures. The novel techniques developed in our laboratory address fundamental properties of compressed materials, e. g. vibrational, electronic, and spin excitations. The presented techniques were made possible both by the 3rd generation synchrotron x-ray sources, and by the development of multiple probes in bench-top experiments with diamond anvil cells. The application of nuclear resonant x-ray technique to the measurements of magnetic transitions and the phonon density of states of iron-containing materials at high pressures will be reviewed with the in-depth discussion of the elasticity of iron and iron oxide at high pressures. Other relevant conventional techniques will be discussed as well, including optical Raman studies of metals under pressure.

Nuclear Resonant Inelastic X-ray Scattering and synchrotron Mössbauer Spectroscopy with Laser-Heated Diamond Anvil Cells

Jung-Fu Lin[1], Wolfgang Sturhahn[2], Jiyong Zhao[2], Guoyin Shen[3], Ho-kwang Mao[1], and Russell J. Hemley[1]
[1]Geophysical Laboratory, Carnegie Institution of Washington, Washington, D.C.
[2]Advanced Photon Source, Argonne National Laboratory, Argonne, IL
[3]Consortium for Advanced Radiation Sources, The University of Chicago, Chicago, IL

The laser-heated diamond anvil cell (LHDAC) technique is a uniquely powerful method for generating the ultrahigh static pressures and temperatures (P>100 GPa and T>3000 K) found deep within planetary interiors. Here we show that the LHDAC technique can be used in conjunction with nuclear resonant inelastic x-ray scattering (NRIXS) and synchrotron Mössbauer spectroscopy (SMS) for studying magnetic, elastic, thermodynamic, and vibrational properties of ^{57}Fe-containing mantle and core materials under high pressures and temperatures. A Nd:YLF laser, operating in continuous donut mode (TEM_{01}), has been used to heat an ^{57}Fe-enriched sample from both sides of a diamond cell. Temperatures of the laser-heated sample are measured by means of spectroradiometry and the detailed balance principle of the energy spectra. The detailed balance principle applied to the inelastic x-ray scattering spectra provides absolute temperatures of the laser-heated sample. Synchrotron Mössbauer spectra of the laser-heated sample are used to reveal magnetic properties under high pressures and temperatures. Sound velocities of iron have been measured up to 70 GPa and 1700 K. We found that temperature has a strong effect on the sound velocities; the compressional (V_P) and shear wave velocities (V_S) of hcp-Fe decrease significantly with increasing temperature under high pressures. The NRIXS measurements in V_S are relatively insensitive to the differences in the EOS data used in deriving the sound velocities. Therefore, the NRIXS technique is particular good at constraining V_S with a precise measurement of the Debye sound velocity (V_D). This study demonstrates a new arsenal of in situ probes to study magnetic, vibrational, elastic, and thermodynamic properties of ^{57}Fe-containing materials, such as metallic Fe, Fe alloys, and iron-bearing oxides and silicates [(Mg,Fe)O and $(Mg,Fe)SiO_3$], in the Earth's interior.

Measuring Velocity of Sound with Nuclear Resonant Inelastic X-Ray Scattering

Michael Y. Hu
Advanced Photon Source, Argonne National Laboratory, Argonne, IL and HP-CAT

Nuclear resonant inelastic x-ray scattering can be used to measure sound velocity of a wide variety of both crystalline and noncrystalline materials, including elemental, composite, and impurity samples. The application of this method to very low concentration of nuclear resonant isotope makes it possible to measure sound velocity of materials which do not contain atomic species of nuclear resonant isotope, assuming uniform doping of the isotope is possible. The sound velocity thus measured is the Debye sound velocity of the sample. In the framework of harmonic solid with Debye-like low-frequency dynamics, a relationship is derived between the low-energy part of measured partial phonon density of states and the sound velocity. This method, when combined with diamond anvil cell and laser heating, has become a valuable tool to understand earth's interior.

Nuclear Resonant X-Ray Scattering of Iron Hydride at High Pressure

Wendy L. Mao[1,4], Wolfgang Sturhahn[3], Dion L. Heinz[1,2], Ho-kwang Mao[1,4], Jinfu Shu[4], and Russell J. Hemley[4]
[1]Department of the Geophysical Sciences, The University of Chicago, Chicago, IL
[2]James Franck Institute, The University of Chicago, Chicago, IL
[3]XOR, Advanced Photon Source, Argonne National Laboratory, Argonne, IL
[4]Geophysical Laboratory, Carnegie Institution of Washington, Washington, D.C.

We studied the nuclear resonant x-ray scattering of iron hydride (FeH_x) up to 52 GPa. Coupled with hydrostatic x-ray diffraction data, the partial phonon density of states measured by nuclear resonant inelastic x-ray scattering provides information on sound velocities and the Fe contribution to thermodynamic parameters. In particular it constrains the aggregate shear velocity and shear modulus for comparison to seismic observations. We found that V_S (km/sec) = 0.023*P (GPa) + 3.2. A loss of magnetism was observed with synchrotron Mössbauer spectroscopy at 22 GPa, lower than theoretically predicted but consistent with the observed anomalous velocity behavior. Results confirm that FeH_x could be a major light element bearing phase for explaining the core density deficit relative to pure Fe. Formation of FeH_x by reaction with water would be expected to leave a signature in the mantle.

Nuclear Resonant Inelastic X-Ray Scattering from ^{83}Kr

J.Y. Zhao
Advanced Photon Source, Argonne National Laboratory, Argonne, IL

We have extended the technique of nuclear resonant inelastic x-ray scattering (NRIXS) to the 9.4035 keV nuclear transition of ^{83}Kr. Development has been made on building monochromators with meV energy-resolution and implementing the microfocusing optics. Energy spectra of nuclear resonant inelastic scattering of ^{83}Kr have been successfully measured on solid Kr at high pressures in diamond anvil cells and on Kr clathrate at low temperatures. Thermodynamic and elastic parameters of krypton are obtained from the measured phonon density of states in these materials.

NRIXS on Kr provides a unique tool that only the Kr guest atoms are measured in Kr clathrates. This allows complete separation of this contribution to the atomic dynamics in the clathrate hydrate. The local modes due to Kr atoms are shown to interact strongly with the molecular lattice cages of water molecules. These interactions are shown to be strong and highly anharmonic in nature. This provides the mechanism for the scattering of acoustic phonons in the clathrate hydrate which is the origin of the glasslike thermal conductivity in these materials.

Iron Valence, Lattice Distortion, and Spin Crossover in (Mg,Fe)SiO_3 Perovskite: A Synchrotron Mössbauer Spectroscopy Study to 120 GPa

Jennifer M. Jackson
Department of Geology, University of Illinois at Urbana-Champaign, IL

The electronic environment of the Fe nuclei in two silicate perovskite samples, $Fe_{0.05}Mg_{0.95}SiO_3$ (Pv05) and $Fe_{0.1}Mg_{0.9}SiO_3$ (Pv10), have been measured to 120 GPa and 75 GPa, respectively, at room temperature using diamond anvil cells and synchrotron Mössbauer spectroscopy (SMS) (sometimes referred to as nuclear forward scattering). Such investigations of extremely small and dilute ^{57}Fe-bearing samples have become possible through the development of SMS. Our results are explained in the framework of the "three-doublet" model, which assumes two Fe^{2+}-like sites and one Fe^{3+}-like site that are well distinguishable by the hyperfine fields at the location of the Fe nuclei. Our results show that at pressures extending into the lowermost mantle the fraction of Fe^{3+} remains essentially unchanged, indicating that pressure alone does not alter the valence states of iron in (Mg,Fe)SiO_3 perovskite. The quadrupole splittings of all Fe sites first increase with increasing pressure, which suggests an increasingly distorted (noncubic) local iron environment. Above pressures of 40 GPa for Pv10 and 80 GPa for Pv05, the quadrupole splittings are relatively constant, suggesting an increasing resistance of the lattice against further distortion. Around 70 GPa, a change in the volume dependence of the isomer shift could be indicative of the endpoint of a continuous transition of the Fe^{3+} from a high-spin to a low-spin state.

Synchrotron Mössbauer Spectroscopy at High Pressure and High Temperature

Guoyin Shen[1], Wolfgang Sturhahn[2], Vitali Prakapenka[1], Jennifer Jackson[3], Jiyong Zhao[2], and Yingwei Fei[4]
[1]Center of Advanced Radiation Sources, The University of Chicago, Chicago, IL
[2]Advanced Photon Source, Argonne National Laboratory, IL
[3]Department of Geology, University of Illinois at Urbana-Champaign, IL
[4]Carnegie Institution of Washington, Washington, D.C.

Mössbauer spectroscopy as a fingerprint technique has been widely used in mineral science. Its applications include characterization of valence state (Fe^{2+}, Fe^{3+}) and spin state of iron, assignment of coordination symmetry, qualitative measure of site distortion, quantitative or semi-quantitative estimation of iron in structurally distinct positions, and correlation of hyperfine parameters with structure variations as a function of pressure and temperature. With the use of brilliant synchrotron radiation, intense x-ray beam can be focused to a size of a few microns. Therefore synchrotron Mössbauer spectroscopy (SMS) offers an ideal tool for studying small materials at extreme pressure-temperature conditions.

Starting from orthopyroxene with composition $Mg_{0.90}Fe_{0.10}SiO_3$, the electronic configuration (valence state and spin state) of iron in its high pressure polymorphs (clinopyroxene, ringwoodite, ilmenite, and perovskite) have been studied using SMS at pressures to 31 GPa and temperatures to 2000 K. The orthopyroxene sample was loaded in a diamond anvil cell. The high-pressure phases were synthesized with laser heating at 1500-2000 K and at pressures of 12 GPa (clino-pyroxene), 19 GPa (ringwoodite), 22 GPa (ilmenite), and 31 GPa (perovskite). Mössbauer spectra were recorded before, during, and after laser heating at each pressure with the newly developed SMS techniques. All phases were identified by x-ray diffraction at room temperature under high pressures.

Data for the orthopyroxene starting material show only Fe^{2+} in two octahedral sites, in agreement with literature data. After compressing the orthopyroxene to 12 GPa, SMS data can be interpreted by Fe^{2+} in a single octahedral site. During heating at 1400 K, Mössbauer spectra show stark difference from that at room temperature. After temperature quench at 12.5 GPa, the transformed clinopyroxene shows Fe^{2+} in a single octahedral site. SMS data for ringwoodite at 19 GPa after heating show weak, yet noticeable, features which may be interpreted as small amount of Fe^{3+}. The similar features become evident at higher pressures for ilmenite and perovskite in which Si is six-coordinated, suggesting large amount of Fe^{3+} in those polymorphs. However, the "Fe^{3+} model" is not the unique interpretation for the observed features. Other models will be discussed, together with implications for the oxidation state of the upper mantle, the transition zone and the lower mantle.

Near Term Prospects for Nuclear Resonant Scattering at the APS*

Esen Ercan Alp
Advanced Photon Source, Argonne National Laboratory, Argonne IL

Nuclear resonant scattering as a tool for investigating properties of materials under high pressures have received very favorable response from the geophysics community at large, despite the fact that the technique itself is undergoing substantial development in terms of instrumentation and data evaluation. This talk will review the recent trends from development point of view and will try to put some perspective for various opportunities at the APS with respect to optics, different isotopes and sample environments.

*Work performed in collaboration with W. Sturhahn, T. Toellner, and J. Zhao, all of Argonne National Laboratory.

This work is supported by US DOE-BES Materials Science under contract number W-31-109-ENG-38.

Nuclear Resonant Scattering on Earth Materials using Synchrotron Radiation

List of Attendees

Nuclear Resonant Scattering 2005

COMPRES

Supported by the
National Science Foundation

Office of Science
U.S. DEPARTMENT OF ENERGY

THE UNIVERSITY OF CHICAGO

ARGONNE NATIONAL LABORATORY

Argonne is operated by The University of Chicago for the U.S. Department of Energy Office of Science

LIST OF ATTENDEES

Alp, Ercan E.
Argonne National Laboratory
Experimental Facilities Division
eea@aps.anl.gov
(630) 252-4775

Bass, Jay D.
University of Illinois
Department of Geology
jaybass@uiuc.edu
(217) 333-1018

Chen, Bin
University of Illinois at Urbana-Champaign
Department of Geology
binchen2@uiuc.edu
(217) 244-8479

Cynn, Hyunchae
Lawrence Livermore National Laboratory
Department of Physics
cynn1@llnl.gov
(925) 422-3432

Sanchez-Valle, Maria del Carmen
University of Illinois at Urbana-Champaign
Department of Geology
csanchez@ens-lyon.fr
(217) 244-1306

Gao, Lili
University of Illinois at Urbana-Champaign
Department of Geology
liligao2@uiuc.edu
(217) 721-7919

Giefers, Hubertus
University of Nevada, Las Vegas
Department of Physics
hubertus@physics.unlv.edu
(702) 895-1718

Hu, Yu (Michael)
Carnegie Institution of Washington
APS/HP-CAT
mhu@hpcat.aps.anl.gov
(630) 252-4078

Jackson, Jennifer M.
University of Illinois at Urbana-Champaign
Department of Geology
jmjackso@uiuc.edu
(217) 333-6379

Lee, Kanani K.M.
California Institute of Technology
Div. of Geological & Planetary Sciences
kanani@gps.caltech.edu
(818) 259-5403

Lerche, Michael
University of Illinois at Urbana-Champaign
Department of Geology
lerche@aps.anl.gov
(630) 252-0964

Li, Jie
University of Illinois at Urbana-Champaign
Department of Geology
jackieli@uiuc.edu
(217) 333-7008

Liebermann, Robert
COMPRES
Robert.Liebermann@stonybrook.edu
(631) 632-1968

Lin, Jung-Fu
Carnegie Institution of Washington
Geophysical Laboratory
j.lin@gl.ciw.edu
(202) 478-8911

Liu, Haozhe
Carnegie Institution of Washington
APS/HP-CAT
hliu@hpcat.aps.anl.gov
(630) 252-4058

Lundin, B. Scott
Massachusetts Institute of Technology
Department of Earth, Atmosphere, and
Planetary Science
slundin@mit.edu
(617) 324-1521

Mao, Ho-kwang (David)
Carnegie Institution of Washington
APS/HP-CAT
mao@gl.ciw.edu
(630) 252-0411

Mao, Wendy L.
The University of Chicago
Department of Geophysical Sciences
wmao@uchicago.edu
(773) 456-6325

Meng, Yue
HPCAT & Carnegie Institution of Washington
Geophysical Laboratory
ymeng@hpcat.aps.anl.gov
(630)252-0483

Prakapenka, Vitali
The University of Chicago
APS/CARS-CAT
prakapenka@cars.uchicago.edu
(630) 252-0439

Scheidt, Robert W.
University of Notre Dame
scheidt.1@nd.edu
(630) 252 -0172

Shen, Guoyin
The University of Chicago
APS/CARS-CAT
shen@cars.uchicago.edu
(630) 252-0429

Song, Maoshuang
University of Illinois at Urbana-Champaign
Department of Geology
mssong@uiuc.edu
(217) 344-1306

Struzhkin, Viktor V.
Carnegie Institution of Washington
Geophysical Laboratory
struzhkin@gl.ciw.edu
(202) 478-8952

Sturhahn, Wolfgang
Argonne National Laboratory
Experimental Facilities Division
sturhahn@aps.anl.gov
(630) 252-0163

Toellner, Thomas S.
Argonne National Laboratory
Experimental Facilities Division
toellner@aps.anl.gov
(630) 252-0166

Tschauner, Oliver
University of Nevada, Las Vegas
Department of Physics
olivert@physics.unlv.edu
(702) 895-1716

Zhao, Jiyong
Argonne National Laboratory
Experimental Facilities Division
jzhao@aps.anl.gov
(630) 252-9195

Nuclear Resonant Scattering on Earth Materials using Synchrotron Radiation

Experiments

Office of Science
U.S. DEPARTMENT OF ENERGY

THE UNIVERSITY OF CHICAGO

ARGONNE NATIONAL LABORATORY

Argonne is operated by The University of Chicago for the U.S. Department of Energy Office of Science

Nuclear Resonant Scattering Workshop 2005

The Phonon Density of States Measured with Synchrotron Radiation and Nuclear Resonances

Wolfgang Sturhahn

Advanced Photon Source, Argonne National Laboratory
9700 South Cass Ave., Argonne, IL 60439

Contents

Overview

In this experiment, we will use synchrotron radiation to measure the density of states of vibrational excitations (phonons.) This technique has been developed over the last decade and is referred to as nuclear resonant inelastic x-ray scattering (NRIXS).[1] Each group of experimenters will conduct a measurement at sector 3-ID of the Advanced Photon Source. We provide support staff to help each group perform the experiment and interpret the data. After data collection (1-2 h per group), the remaining time will be spent with evaluation and interpretation. In addition to your own data, we provide similar sets of data. Computer hardware (PCs running as X-terminals) and software for data manipulation will be provided. It is important that you understand the basic principles of the experimental method. Therefore we strongly recommend that you read the next section and the attached article *Phonon Density of States Measured by Inelastic Nuclear Resonant Scattering*. You are expected to use this description to familiarize yourself with the experimental setup and its individual components before the start of the experiment. You should be able to solve at least 75 % of the quiz correctly. If you have particular questions or a general problem in understanding this document, please contact Dr. W. Sturhahn, Bldg. 431, Rm. D007, tel. 0163.

Principles of the Method

In this chapter, we will discuss the basic properties of a nuclear resonance and its connection to atomic vibrations. In a study of the "Table of Isotopes," one can find several stable isotopes that have the first excited state at energies of a few keV. Such isotopes can be excited with x rays, and observation of the scattering products reveals information about the nuclear resonance and its environment. In our experiment, we will work with the ^{57}Fe isotope, which has a nuclear resonance at 14.4125 keV. A copy of the nuclear level scheme of ^{57}Fe is attached. The natural abundance of ^{57}Fe is about 2 %, and we find numerous examples in technology, material science, life sciences, and environmental science, where iron compounds are of importance. The unique aspect of using resonant isotopes to measure phonon energies is mainly the selectivity. This means that vibrations can be probed locally in systems that have resonant isotopes in specific places, e.g., biomolecules like myoglobin, thin films, and materials under extremely high pressure (>100 GPa.)

An important property of the nuclear resonance is the energy width of the excited state or natural line width. For ^{57}Fe we find the very small value of $\Gamma = 4.66$ neV. Only x-ray sources with high spectral intensity have a reasonable chance of exciting the nucleus. A nucleus, once excited, decays with its natural lifetime of $\tau = \hbar/\Gamma = 141$ ns. Even though the level width is small, the nuclear resonant cross section is large. We have $\sigma = 2.56$ Mb,

[1] The terms "nuclear resonant vibrational spectroscopy (NRVS)" and "nuclear inelastic scattering (NIS)" are also used in the literature.

which is 450 times larger than the cross section for photoelectric absorption by the atomic shell.

The understanding of nuclear resonant scattering is much simplified by the ratios of the involved energy scales

$$\text{transition energy (keV)} \longleftrightarrow \text{phonon energy (meV)} \longleftrightarrow \text{nuclear level width (neV)} \quad .$$

The energies are different by six orders of magnitude. Figure 1 illustrates this peculiar situation in more detail. In panel (a), the nucleus is held fixed, i.e., we neglect recoil from

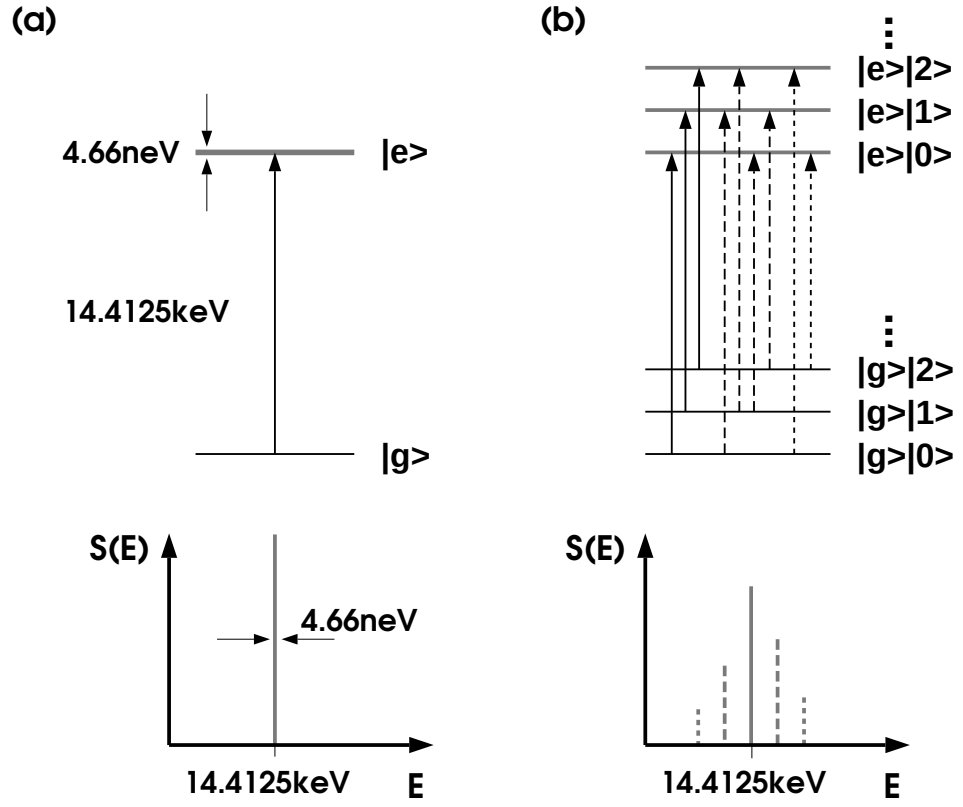

Figure 1: The influence of atomic vibration on the nuclear level scheme. Panel (a) shows the energy levels of a fixed ^{57}Fe nucleus. When x-rays interact with materials containing ^{57}Fe the nuclear transition $|g\rangle \rightarrow |e\rangle$ causes a sharp resonance in the excitation probability density $S(E)$. The nucleus embedded in an Einstein solid has the more complex level scheme shown in panel (b). In addition to the peak at the nuclear transition energy, $S(E)$ now features side bands. The dashed lines show transitions that include creation or annihilation of one phonon with the Einstein energy. Transitions that involve more phonons are also possible, e.g., the dotted lines describe two-phonon creation/annihilation.

photon absorption, and only x-ray photons within width Γ around the transition energy

can excite the resonance. This behavior is quantitatively described by the excitation probability density $S(E)$, and the cross section for a particular scattering channel is proportional to $S(E)$. The value of $S(E)dE$ gives the probability that the nucleus can be excited by x rays in the energy range $[E, E+dE]$. If the nucleus is allowed to oscillate with a particular frequency (the Einstein model of a solid), the picture changes dramatically. Panel (b) of Fig. 1 illustrates the new energy levels that evolve from combinations of nuclear states and phonon states, e.g., $|g\rangle|1\rangle$ is a quantum state with the nucleus in the ground state and one phonon present. The small coupling between nucleus, phonon, and x-ray photon and the different energy scales mentioned before make such states very good approximations of the exact eigenstates of the coupled system. In a real material, phonons with many different energies exist, and the side bands in $S(E)$ become smeared out. However, the classification into one-phonon, two-phonon, etc., events remains valid. If the incident x-ray energy is too small to excite the nuclear resonance directly, phonons have to be annihilated. This process will always be less likely than the creation of phonons with the same energy. The ratio is given by the Boltzmann factor, i.e., $S(E) = \exp[E/k_BT]\, S(-E)$ with temperature T and Boltzmann's constant k_B. At zero temperature the effect is

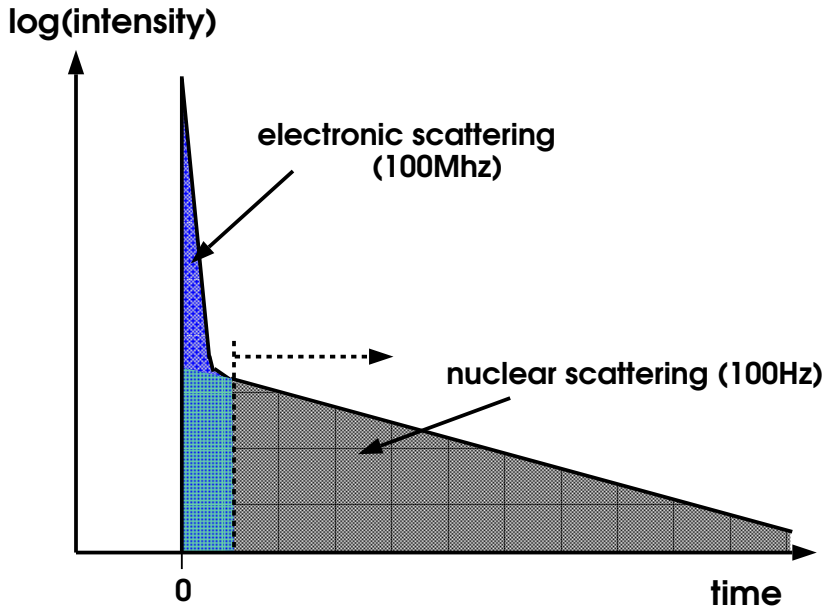

Figure 2: Scattered intensity vs. time after excitation. At time zero, a synchrotron radiation pulse excites a material containing a nuclear resonant isotope. The scattering from electrons is prompt, i.e., almost immediately after the pulse arrived. The response of the resonant nuclei is delayed. Time discrimination permits to distinguish nuclear and electronic scattering.

extreme because phonon annihilation becomes impossible, and $S(E)$ has only one sideband at positive energies.

If we can measure the probability of exciting a nucleus, we can derive $S(E)$, which contains all the phonon energies. Let us imagine a nucleus that was excited by some process. The nucleus will try to decay into the ground state either by emission of an x-ray photon of approximately 14.4125 keV or by transfering the excitation energy to the electron shell. In the latter case, an electron is expelled (most likely from the K-shell), and the hole is quickly filled by other electrons under the emission of fluorescence x rays. All these decay products are emitted with some delay relative to the time of excitation, and the average time is given by the natural life time of 141 ns. Figure 2 shows the scattered intensity of a material containing a nuclear resonance after excitation with a synchrotron radiation pulse. Scattering of x rays from electronic charge is very fast ($< 10^{-12}$ s). If the energy of the incident x rays is close to the nuclear transition energy, nuclei are excited, and delayed emission of x rays can be observed. If only the delayed photons are counted while tuning the energy of the incident x-ray pulses, we expect to measure a function that is proportional to $S(E)$. The time discrimination removes all non-nuclear scattering of the x rays very effectively. $S(E)$ is obtained from the measured data by proper normalization, and the partial phonon density of states can be extracted by a mathematical procedure. Both steps are explained in the attached paper *Phonon Density of States Measured by Inelastic Nuclear Resonant Scattering*. The word "partial" refers to the selection that has taken place by observing only vibrations at the positions of the resonant isotope.

Setup and Components

The experimental setup can be broken down into several components. A schematic is shown in Fig. 3. At the beginning of the experiment all components will be aligned and functional. However, we require you to be familiar with the purpose and functionality of each component as described in this manual. The x-ray source are electrons that are orbiting in the storage ring and periodically (once per turn) pass through an undulator. The x rays are monochromatized in two steps (premonochromator and high-resolution monochromator) to an energy bandwidth that is more narrow than the phonon spectrum of our samples. The monochromatized x rays excite nuclear resonances in the sample. The re-emitted radiation is observed with the detector. The timing circuit measures the elapsed time between excitation and re-emission and removes prompt events. The control unit permits us to remotely interact with devices that are inside the radiation area and thus are not directly accessible during the measurement.

X-ray source

We use synchrotron radiation as the source for x rays. Synchrotron radiation is created by charged particles that are stored on closed orbits. To keep the particles on closed orbits they have to be accelerated perpendicular to their propagation direction. At the

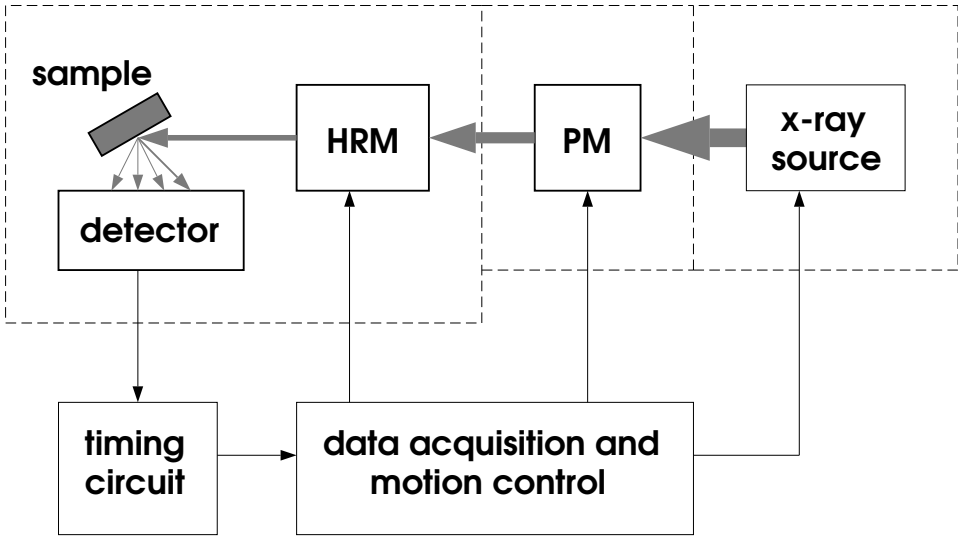

Figure 3: Setup of the experiment. Grey lines indicate x-rays. Solid lines symbolize flow of data or control information. PM and HRM abbreviate premonochromator and high-resolution monochromator, respectively. The dashed lines indicate enclosures with lead walls that protect experimenters from exposure to the x-rays. The components are described in the text.

Advanced Photon Source electrons with an energy of 7 GeV are kept on an approximately circular orbit with a circumference of about 1.1 km (0.7 miles). The electrons are highly relativistic, and they need 3.68 μs for one turn. On average it takes about 10^{11} turns or 20 hours before an electron is lost by being scattered from its stable orbit. If left alone the stored electrons would slowly disappear from the orbit and the x-ray intensity would decrease. Therefore scientists at the Advanced Photon Source have developed a scheme to compensate for this loss every few minutes automatically. This operation mode is called "top-up" mode. Other storage rings have to be periodically refilled.

The magnets that keep the electrons in the orbit are called bending magnets. The x rays produced at the bending magnets are moderately intense. Much more intense x rays are obtained from undulators, which are devices with a spatially periodic magnetic field. The electrons propagate through the field and experience small periodic deviations from a straight line. The accelerations exerted by the periodic field lead to the emission of very collimated and intense x rays. In the experiment, we use such an undulator to obtain the required spectral intensity (remember the narrow width of the nuclear resonance).

The electrons are not randomly distributed in the storage ring but may occupy a finite number of stable orbits. These stable orbits are called buckets, and there are 1296 buckets separated by 0.85 m or 2.84 ns. Buckets that are filled with electrons are called bunches, and we call the actual pattern of bunches the time structure of the synchrotron radiation. The standard time structure at the Advanced Photon Source is shown in Fig. 4. It is very

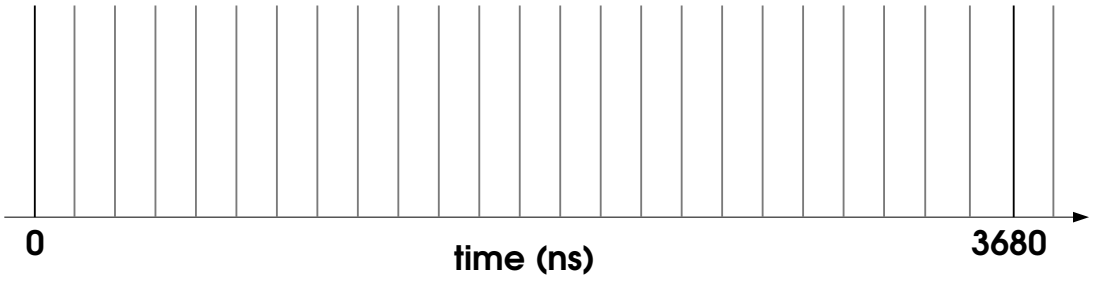

Figure 4: Standard time structure at the Advanced Photon Source. Vertical lines indicate the bunch positions. The total number of bunches is 24 and they are separated by 153.3 ns. The bunch pattern is periodic and is repeated after 3680 ns, the time it takes an electron with 7 GeV energy to complete the orbit. Each bunch contains 4.25 mA current.

important for nuclear resonant scattering experiments that the time between bunches (153 ns) is larger than the dead time of the detector (20 ns.) The bunches are filled with about 10^{11} electrons corresponding to an average current of 4.25 mA.

The size of a bunch is 0.036 mm vertical, 0.56 mm horizontal, and 20 mm along the direction of propagation. The transverse size of the bunch determines the size of the x-ray source. Each bunch produces an x-ray pulse when passing through the undulator. The bunch length gives 70 ps duration for each x-ray pulse. Another important parameter is the divergence or angular width of the produced radiation. The divergence increases the size of the x-ray beam with larger distance from the undulator. We have divergences of 9 μrad vertical and 34 μrad horizontal. The sample is mounted at 35 m distance from the x-ray source (undulator). This distance results in a beam size of $0.35 \times 1.75\,\mathrm{mm}^2$.

Premonochromator

The undulator creates a broad energy band of x rays (the so-called "white beam") that ranges from about 6 keV up to several 100 keV, even though there are distinct peaks with enhanced intensity and widths of about 200 eV. The premonochromator filters an energy band of about 1 eV from the white beam. This bandwidth is not narrow enough to perform phonon spectroscopy (remember that phonon energies are typically less than 0.1 eV) but the total power in the x-ray beam is reduced from 1000 W to 0.1 W. The reduction in power is important because the high-resolution monochromator is very sensitive to temperature gradients (see next section). Two diamond crystals in nondispersive arrangement (like a "channel cut") operate at their (111) Bragg reflections to perform the task of filtering and power reduction. Diamond is a very suitable material because its excellent thermal conductivity and low absorption for x rays. Each crystal's size is about $7 \times 5 \times 0.35\,\mathrm{mm}^3$. In the experiment, the premonochromator is adjusted to transmit around the nuclear resonance energy of 14.4125 keV. Also the undulator is tuned to produce an intense peak at this energy. The spectral photon flux after the premonochromator is 10^{13} photons/s/eV

at 100 mA storage ring current.

High-resolution monochromator

In order to carry out your experiment, it is necessary to reduce the energy bandwidth to a level that will allow you to resolve vibrational excitations that range in energy from 0 to say 100 meV. For this purpose, you will use a high-resolution mononchromator that reduces the energy bandwidth of the x rays to approximately 1 meV and has a tunability range that can easily cover the ±100 meV energy range around the nuclear resonance where the probability for phonon excitation or annihilation is high.

The principle of high-resolution monochromatization in this region of the electromagnetic spectrum relies upon the use of Bragg diffraction from a series of perfect single crystalline materials. Pure single-crystalline silicon is the material most often used for this purpose because it is commercially available in large boules of extremely high quality. The high-resolution monochromator schematically shown in Fig. 5 will be the one used in your experiment. The orientation of the four crystals is such that they will all be Bragg-diffracting the 14.4125 keV x rays from a pre-chosen set of diffraction planes. These diffraction planes and their orientation with respect to the crystal surfaces are chosen to achieve optimal performance in terms of efficiency and energy resolution and are selected when the monochromator is fabricated.

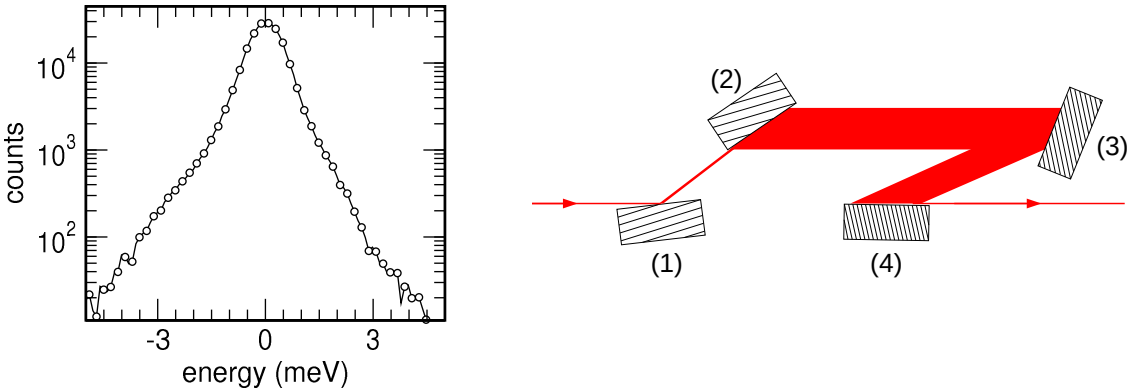

Figure 5: Design (right) and resolution function (left) of the high-resolution monochromator for 14.4125 keV x-rays. The first and second crystal faces use silicon (4 0 0) reflections, and the third and forth faces use silicon (10 6 4) reflections. Note that the diffraction planes are not parallel to the crystal surfaces. The resolution function was measured with coherent elastic nuclear resonant scattering relative to the nuclear transition energy.

The operation of the high-resolution monochromator will be relatively straightforward for this experiment since it will be pre-aligned for you. During the experiment, though, the high-resolution monochromator needs to be scanned in energy by changing the angles

that the x rays include with each crystal face. Also, the spacing of the diffraction planes depends upon the temperature, so any changes in the temperature of each crystal needs to be recorded. Crystal faces 1,2 and 3,4 are each part of an assembly that is called "artificial channel cut" and consists of two individual crystals using the same Bragg reflections mounted on the axis of a ultra-high resolution goniometer. Thus, there are only two rotation angles that need to be controlled. Calibration of the energy scale forms a critical aspect of the measurement, and the conversion from relative rotation angle and temperature of the two crystals to relative energy is given by

$$\delta E = E_o \, \frac{\delta\theta_1 - \delta\theta_2 - \alpha \left(\delta T_1 \tan\Theta_1 + \delta T_2 \tan\Theta_2\right)}{\tan\Theta_1 + \tan\Theta_2} \ , \tag{1}$$

where the energy, angles and temperatures are referenced from their values at the nuclear transition energy. The nominal Bragg angles of the crystal pairs are given by $\Theta_1 = 18.5°$ and $\Theta_2 = 75.2°$, the temperature of the i^{th} crystal is depicted by T_i, the coefficient of thermal expansion α has the value $2.56 \times 10^{-6}\, K^{-1}$ for silicon near room temperature, and $E_o = 14.412497\,\mathrm{keV}$.

In order to take high-quality spectroscopic data, it is necessary to know the energy response of your instrument. In the case of inelastic nuclear resonant scattering with synchrotron radiation, energy response is determined solely by the high-resolution monochromator. The energy resolution function of the monochromator can be measured using coherent elastic nuclear resonant scattering [2] and is used in the evaluation process of your inelastic data. You will be provided with the resolution function of the monochromator. An example of an energy resolution function for a high-resolution monochromator is given in figure 5.

Detector and timing circuit

We discussed earlier how the nuclear resonant signal is discriminated by timing technique (see Fig. 2). We need a detector with a very good time resolution, say 1 ns. Also an excellent dynamic range is required, i.e., after the intense pulse of prompt photons the detector has to quiet down in a reasonably short time, say 10 ns. The best x-ray detectors with such qualities are avalanche photodiodes or APDs. The APD is a semiconductor device made from silicon. It consists of a p-n junction that is operated under reverse bias. The electric fields in a region around this p-n junction are high enough to amplify a small current from impact ionization, e.g., absorption of an x-ray photon. This so called "active region" is about 100 μm thick. The active area of the APD is $10\times10\,\mathrm{mm}^2$. Figure 6 shows a circuit diagram and a picture of the actual detector. The detector produces negative signals of a few ns duration. The height of the pulse depends on the x-ray energy. For a 14.4 keV photon, the average pulse height is about 200 mV on 50 Ω. The time resolution

[2] This is the same type of scattering that is used for synchrotron Mössbauer spectroscopy.

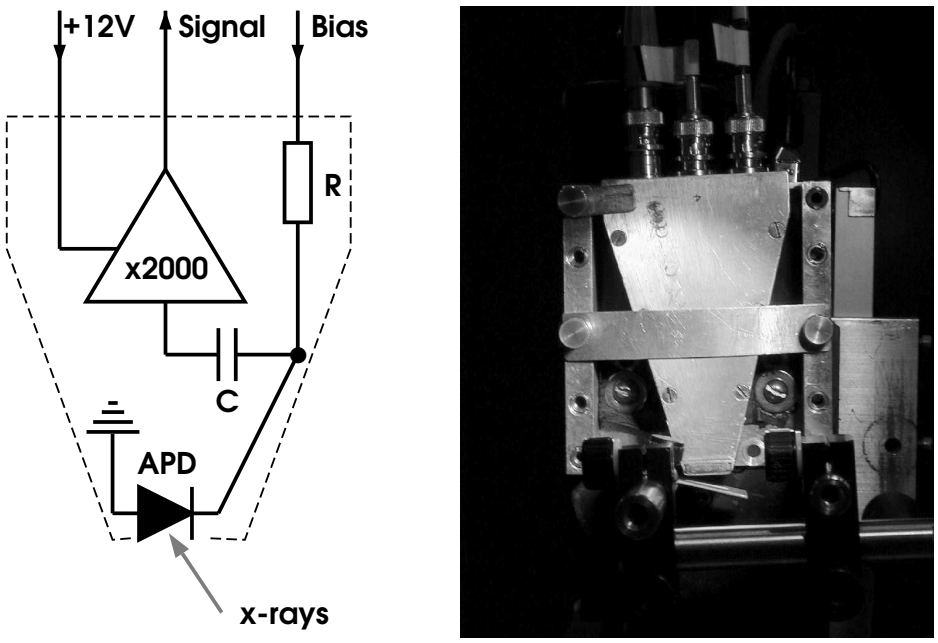

Figure 6: Circuit diagram of the APD-detector (left) and picture of the actual device (right). The bias voltage varies with the particular APD around typically 300 V. Other typical values are $R = 10\,M\Omega$ and $C = 100\,pF$. The signal following the absorption of a 14.4 keV photon is a negative pulse of 3 ns duration and an average height of 200 mV on $50\,\Omega$.

of this detector is about 1 ns.

Additional electronic components are needed to discriminate between prompt and delayed x rays. First we need to know when the x-ray pulses arrive at the sample. We learned in the section about the x-ray source that x-ray pulses will be synchronized with the bunch pattern in the storage ring. The bunch pattern can be derived electronically from the operation parameters of the storage ring. The device that performs this task is called the bunch clock generator. It provides us with a sequence of electronic pulses that looks just like Fig. 4. The timing circuit will compare the output signal of the APD detector with the signal from the bunch clock generator. Panel (a) in Fig. 7 shows the circuit. The anti-coincidence unit filters out the delayed events. The timing diagram is displayed in panel (b). Different experimental situations are accommodated by the adjustable width and delay time of the output pulses of the bunch clock generator. Besides delayed events that originate in nuclear resonant scattering, electronic noise may fake "delayed events" because such pulses are asynchronous with the bunch pattern. Electronic noise created by the detector is unavoidable but, for our APD detectors, sufficiently small. Usually 0.03 cps are caused by noise. The noise events will be independent of the energy of the incident x rays (remember that the nuclear delayed event will strongly depend on the

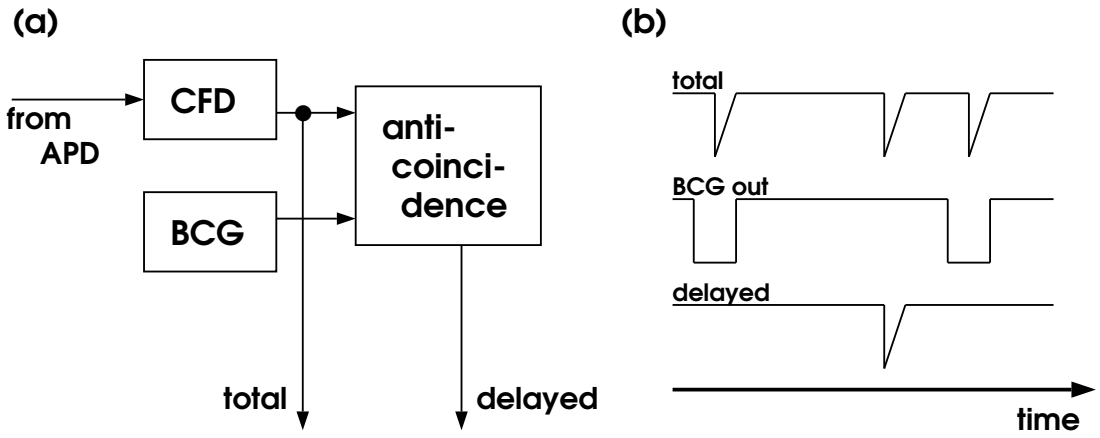

Figure 7: Timing circuit for the discrimination of prompt and delayed photons. The analog signal from the APD-detector is converted to a digital NIM-signal by the constant-fraction discriminator (CFD.) An anti-coincidence logic blanks out the prompt signals that arrive synchronously with the bunch clock generator (BCG) output. Only delayed pulses remain as output signal. The timing diagram is shown in panel (b).

incident energy) and can be measured by tuning the incident x-ray energy sufficiently far off resonance.

Experimental Procedure

First and foremost, think before you act. Familiarize yourself with the beamline setup. The experiment to be performed will involve measuring the nuclear resonant absorption probability of different materials around the 14.4 keV nuclear resonance using the technique of nuclear resonant inelastic x-ray scattering (NRIXS). You will perform this measurement on three different ^{57}Fe-containing compounds, iron metal, stainless steel ($Fe_{55}Cr_{25}Ni_{20}$), and hematite (Fe_2O_3.) Naturally occurring iron only contains 2% of ^{57}Fe, the rest being predominantly ^{56}Fe. The samples you will measure are enriched to greater than 95% ^{57}Fe to increase your signal so that you may complete the measurements in the alloted time.

Performing the measurement will involve measuring the yield of nuclear resonant photons as a function of incident x-ray energy. To measure the photons you will use an avalanche photodiode detector that is placed as close as possible to the scattering volume. Due to the 141 ns lifetime of the 14.4 keV nuclear excited state, the nuclear resonant photons are "delayed" relative to the nonresonant, or "prompt", photons. Timing electronics are used to separate the nuclear resonant delayed photons from the nonresonant prompt photons. The timing electronics will be set up beforehand, but you should understand the impor-

tance of the time-filtering technique, as well as the essential properties of the detector that motivates one to choose it over other detectors. The energy of the x rays incident on the sample is varied by rotating the crystals of the high-resolution monochromator. To change the energy transmitted by the monochromator by 1 meV, you need to rotate the (4 0 0) crystal by 0.023 μrad and the (10 6 4) crystal by 0.29 μrad. Note that temperature changes of the high-resolution monochromator will also alter the transmitted x-ray energy in accordance with equation 1, so thermal stability of the monochromator is also important. You should record the crystal angles as measured by the number of pulses transmitted to the stepper motors controlling the rotation axes, as well as the temperatures of the crystals as measured by thermal sensors at *every* step of the energy scan. This will allow you to reconstruct the energy scale later by using Eq. (1).

Nearly everything in the experimental hutch is remotely controlled by computer software. The crystal angles can be scanned with the use of the computer. In addition, you should setup the computer to have all the necessary experimental parameters (angles, temperatures, countrates, etc.) written to a data file. In addition, there are many sensors/detectors/monitors that allow one to track the state of the x-ray beam, the optics, and the experiment itself. Some of these need to be checked before the experiment can be performed. The following is a small checklist that you should go through to ensure that you collect usable data.

Checklist for collecting data

1. Beam should be stable
   - $\longrightarrow \leq 5\,\mu$rad vertical angle
   - $\longrightarrow \leq 25\,\mu$rad horizontal angle
   - $\longrightarrow \leq 100\,\mu$m vertical position
   - $\longrightarrow \leq 100\,\mu$m horizontal position

2. Premonochromator should be aligned properly
   - $\longrightarrow$ counting rate (flux) after premono should be optimized with a drift of $\leq 5\%$/hr

3. High-resolution monochromator (HRM) should be aligned properly
   - $\longrightarrow$ maximize flux after HRM by rotating the crystals while maintaining the energy alignment
   - $\longrightarrow$ move energy of HRM to nuclear resonance energy and optimize delayed counting rate
   - $\longrightarrow$ counting rate (flux) after HRM should have a drift of $\leq 5\%$/hr

4. Timing electronics should be set properly
   - $\longrightarrow$ move energy of HRM 200 meV below the nuclear resonance energy and measure background (delayed) counting rate in the APD detector: should be ≤ 0.03 cps

$\longrightarrow$ move energy of HRM back to nuclear resonance energy

5. Scan parameters should be set properly

   $\longrightarrow$ scan range should be properly centered and extending at least $\pm 100\,\mathrm{meV}$
   $\longrightarrow$ energy step size should be approximately one third of the energy bandwidth of the HRM
   $\longrightarrow$ counting time per energy step should be adjusted to produce an hour-long scan
   $\longrightarrow$ check that all relevant experimental parameters necessary to evaluate the data are being written to the data file: motor positions, crystal temperatures, delayed counts, incident intensity on sample etc.

Additional Reading

- The study of the following material is strongly recommended.

  1. W. Sturhahn et al., *Phonon Density of States Measured by Inelastic Nuclear Resonant Scattering*, Phys.Rev.Lett. **74**, 3832 (1995)
  2. W. Sturhahn, *Nuclear Resonant Spectroscopy*, J. Phys.: Condens. Matter **16**, S497 (2004)

- These texts provide a good source of supplementary information.

  1. Phonons in general :
     N.W. Ashcroft and N.D. Mermin, *Solid State Physics*, (W.B. Saunders Company, Philadelphia, PA, 1976)
  2. Inelastic x-ray scattering in general :
     E. Burkel, *Phonon spectroscopy by inelastic x-ray scattering*, Rep.Prog.Phys. **63**, 171 (2000)
  3. Nuclear absorption :
     K.S. Singwi and A. Sjölander, *Resonance Absorption of Nuclear Gamma Rays and the Dynamics of Atomic Motions*, Phys.Rev.**120**, 1093 (1960)
  4. Procedure of data evaluation :
     M.Y. Hu et al., *Data Analysis for Inelastic Nuclear Resonant Absorption Experiments with Synchrotron Radiation*, Nucl.Instrum.Methods A **428**, 551 (1999)
  5. Software for data evaluation :
     W. Sturhahn, *CONUSS and PHOENIX: Evaluation of Nuclear Resonant Scattering Data* Hyperfine Int. **125**, 149 (2000)

- More details can be found in the following papers.

1. Monochromators :
   T.S. Toellner, *Monochromatization of synchrotron radiation for nuclear resonant scattering experiments*, Hyperfine Int. **125**, 3 (2000)
2. Theory :
   W. Sturhahn and V.Kohn, *Theoretical Aspects of Inelastic Nuclear Resonant Scattering*, Hyperfine Int. **123/124**, 367 (1999)
3. Experiment :
   A.I.Chumakov and W.Sturhahn, *Experimental Aspects of Inelastic Nuclear Resonant Scattering*, Hyperfine Int. **123/124**, 781 (1999)
4. Sound velocity extraction :
   M.Y. Hu et al., *Measuring velocity of sound with nuclear resonant inelastic x-ray scattering*, Phys.Rev. B **67**, 094304 (2003)

Quiz

The following short quiz tests how carefully you have read the given material and sometimes a little more. You should be able to answer 75 % or so correctly. We will discuss the answers before or during the experiments.

1. What is the abundance of the element iron in Earth's crust ?
2. Why is the planned experiment selective to ^{57}Fe ?
3. What are energy and lifetime of the first nuclear excited state of ^{57}Fe ? What are energy and lifetime of an excited Fe atom with a hole in the K-shell ?
4. Why is the nuclear resonant cross section so large ?
5. Imagine the resonant isotope embedded in an isotropic Debye solid (see Fig. 1 for the case of the Einstein solid.) What are the width and the height of the peak in $S(E)$ that occurs at the exact nuclear transition energy ?
6. We normalize our data using the first moment instead of the zeroth moment (area). Why can't we simply use area normalization to obtain $S(E)$ from our data ?
7. Many solids behave like a collection of coupled harmonic oscillators, and $S(E)$ can be expressed as sum of n-phonon contributions ($n = 0, 1, \ldots$) Calculate the one-phonon contribution $S_1(E)$ for the Debye model. Give the functional dependence of $S_1(E)$ for $E \ll k_B T$.
8. Why can't we use an x-ray tube for our experiment ?
9. What is the task of the premonochromator ?

10. Compare the power density (W/mm^2) of white beam at 25 m from the undulator and sunlight in Chicago in summer.

11. Why is the overall energy resolution only determined by the high-resolution monochromator ?

12. Equation (1) implies that we can change $\delta\theta_1$ and $\delta\theta_2$ without changing the energy. What does this mean ?

13. Why do we need the resolution function of the monochromator ?

14. What are the properties that make APDs suitable detectors for our experiment ? Do we need energy resolution in the detector ?

15. Calculate the temperature change (assume the same value for both crystals) that is needed to shift the energy of the high-resolution monochromator by 1 meV.

16. Why is it better to move the HRM 200 meV below (rather than above) the nuclear resonance energy to measure the background ?

Phonon Density of States Measured by Inelastic Nuclear Resonant Scattering

W. Sturhahn, T. S. Toellner, and E. E. Alp
Advanced Photon Source, Argonne National Laboratory, Argonne, Illinois 60439

X. Zhang and M. Ando
Photon Factory, National Laboratory for High Energy Physics, Oho 1-1, Tsukuba, Ibaraki 305, Japan

Y. Yoda and S. Kikuta
Department of Applied Physics, Faculty of Engineering, The University of Tokyo, Hongo 7-3-1, Bunkyo-ku, Tokyo 113, Japan

M. Seto
Research Reactor Institute, Kyoto University, Sennan-gun, Osaka 590-04, Japan

C. W. Kimball and B. Dabrowski
Department of Physics, Northern Illinois University, De Kalb, Illinois 60115
(Received 16 December 1994)

The phonon density of states was measured by observing the nuclear resonant fluorescence of ^{57}Fe versus the energy of incident x rays from a synchrotron radiation beam. An energy resolution of 6 meV was achieved by use of high-resolution crystal optics for the incident beam. Extremely low background levels were obtained via time discrimination of the nuclear fluorescent radiation.

PACS numbers: 63.20.–e, 76.80.+y

Knowledge of the dynamics of atomic motion has been valuable in condensed matter physics [1]. It is possible to obtain this information by measurement of the phonon dispersion relation with slow neutrons or monochromatic light, the latter with a very restricted range in momentum transfer, along different directions of a single crystalline sample [2,3]. The data can be used to reconstruct the complete four-dimensional dispersion surface once a specific model for the interatomic forces has been chosen. The phonon density of states (DOS) is then calculated from the reconstructed dispersion relation [4]. In many cases of interest, single-crystal samples are not available or it might be sufficient to know the phonon DOS and not the complete dispersion relation. This situation can be accommodated by collecting the scattered neutrons over a large solid angle for those elements with an appreciable cross section for inelastic neutron scattering. The energy of the scattered neutrons has to be determined, e.g., by time-of-flight analysis, and the selected neutrons have to be discriminated against electronic scattering contributions and detector noise. The scattering of x rays was considered as an alternative method to analyze excitations in solids [5]. The x rays interact predominantly with the electrons in the solids, and vibrational excitations are accompanied by low energy electronic excitations.

In the present Letter, we use a recently reported method [6] that permits derivation of the phonon DOS directly from the measured data. We observed the absorption of x rays from the 14.4136-keV nuclear resonance of ^{57}Fe and the subsequent deexcitation by emission of K-fluorescence radiation. Nuclear resonances that are low in energy usually have a very narrow energy width, 4.66 neV for ^{57}Fe. Considering inelastic scattering, we may benefit from such a well-defined energy reference in the lattice. This allows tuning the energy of the incident x rays with respect to this resonance and not with respect to the energy of the scattered particle, which then would have to be determined. Furthermore, the deexcitation of the nucleus by emission of a conversion electron followed by fluorescence radiation takes place on a time scale of the lifetime of the nuclear resonance, 141 ns for ^{57}Fe. If the nucleus is excited by pulsed synchrotron radiation, the discrimination of nuclear resonant absorption from the electronic contribution is very efficiently done by counting only delayed fluorescence photons. Tuning the energy of the incident synchrotron radiation with respect to the nuclear resonance while monitoring the total yield of the delayed fluorescence photons gives a direct measure of the phonon DOS.

Nuclear resonances with low transition energies on the order of 10 keV can be coherently excited by synchrotron radiation with very high efficiency [7–9]. Besides the precise determination of hyperfine interaction parameters, these experiments permit determination of the Lamb-Mössbauer factor [10,11]. The incoherent scattering from a nuclear resonance was observed [12,13], but the signal was too weak for further analysis. The probability of such a process can be calculated from a self-correlation function of the displacement of the nucleus. Similar self-correlation functions were discussed earlier with respect to neutron scattering [14] and with respect to effects on the line shape of the nuclear resonance in Mössbauer transmission experiments [15]. The quantitative analysis gives reasonable

 0031-9007/95/74(19)/3832(4)$06.00

probability for the excitation of the nuclear resonance with synchrotron radiation when the energy is tuned away by an amount needed for creation or annihilation of phonons. The arrival of a very short (<100 ps) synchrotron-radiation flash triggers the emission process of an inelastically scattered photon or of a conversion electron and subsequent fluorescence radiation. In both cases the delay of this emission is on the order of the natural lifetime of the nuclear resonance. The discrimination of the delayed events, which then signal the creation or annihilation of phonons from all other scattering contributions, which are prompt in time, is achieved by conventional timing methods. The energy resolution in the phonon spectrum is determined by the energy bandwidth of the incident synchrotron radiation.

In the present experiment, the 14.4136-keV resonance of the Mössbauer isotope ^{57}Fe was employed because of its large resonance cross section, the tolerable electronic absorption in the materials used, and the convenient lifetime. However, the method can be applied for any nuclear resonance of nuclei in solids, liquids, or gases.

The experiments were performed at the undulator beamline NE#3 at the 6.5-GeV KEK-AR synchrotron radiation facility in Tsukuba, Japan [16]. A high-heat-load monochromator, which consists of two symmetric silicon (111) reflections in a nondispersive setting, and a high-resolution, nested monochromator, as described earlier [17], were employed to achieve the required energy resolution. The high-resolution monochromator uses asymmetric silicon (422) and symmetric silicon (10 6 4) reflections. The synchrotron radiation incident on the ^{57}Fe-containing sample had an energy bandwidth of 6 meV at 14.4136 keV. An avalanche photodiode (APD) with an active area of 2 cm^2 was used to detect the emitted fluorescence radiation [18]. The photon flux on the sample was monitored with an ion chamber for proper normalization of the data.

The time delay between the output pulses of the APD detector and the bunch arrival signal that was derived from the RF of the storage ring was measured. The nonresonantly scattered radiation that appears promptly with respect to the bunch arrival signal was eliminated by counting in a time window of 30 to 600 ns after the arrival of the synchrotron radiation flash. The detector noise in this time window was less than 0.03 Hz. The energy of the incident radiation was tuned by rotating the (10 6 4) channel-cut crystal in steps of 1.55 meV. The samples were mounted at a distance of $\approx$3 mm from the APD with an inclination angle of $\approx$10° relative to the incident beam providing good coverage of solid angle and illuminating a large sample volume.

We observed phonon spectra from metallic foils of α-iron and stainless steel $Fe_{0.55}Cr_{0.25}Ni_{0.2}$ with thicknesses of 10 and 30 μm, respectively. In addition, phonon spectra were taken from powder samples of strontium iron oxide, $SrFeO_x$ with $x = 2.5, 2.74, 2.86, 3.0$ and sample thicknesses of about 100 μm. The measurements were conducted at room temperature (298 K), and the samples were 95% enriched in ^{57}Fe. The collection time for each phonon spectrum ranged between 50 (stainless steel) and 100 min ($SrFeO_x$).

The main features of the observed phonon spectra are an elastic peak and sidebands at lower and higher energy (inset of Fig. 1). The elastic peak dominates the spectrum, as expected for solids with reasonable probability for recoilless absorption. Photons with less energy can excite the nuclear resonance by annihilation of a phonon (low energy sideband). The high energy sideband corresponds to phonon creation. Phonon annihilation is proportional to the temperature-dependent phonon occupation number, whereas the creation of phonons can also occur spontaneously, which explains the observed asymmetry in the spectra.

With the energy of the incident synchrotron radiation shifted by E relative to the nuclear resonance, the flux of delayed K-fluorescence photons emitted in the full solid angle is given by

$$I(E) = I_0 \rho \sigma \frac{\eta_K \alpha_K}{1 + \alpha} \frac{\pi}{2} \Gamma S(E), \qquad (1)$$

where I_0 is the incident photon flux, σ is the nuclear resonant cross section, η_K is the fluorescence yield, α, α_K are the total and partial internal conversion coefficients, respectively, and Γ is the nuclear level width. The effective area density of nuclei ρ also accounts for absorption within the material. $S(E)$ is the absorption probability per unit of energy. We will give it in terms of the quantum states $|\chi\rangle$ and the displacement operator $\hat{\mathbf{r}}$ of the nuclear motion

$$S(E) = \left\langle \frac{1}{dE} \sum_n |\langle \chi_n(E) | e^{-i\mathbf{k}\cdot\hat{\mathbf{r}}} | \chi_i \rangle|^2 \right\rangle_i . \qquad (2)$$

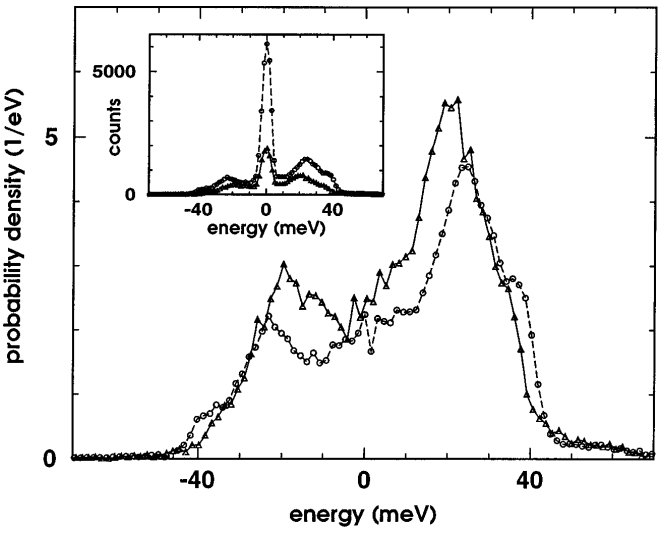

FIG. 1. The absorption probability density $S(E)$, as given in Eq. (2), is shown for α-iron (circles, dashed line) and stainless steel (triangles, solid line). The elastic peak is removed as described in the text. The inset shows the raw data.

The sum is over those intermediate states that differ by energies in the interval $[E, E + dE]$ from the initial state, and a thermal average is performed over the initial state. $\mathbf{k}$ is the wave vector of the incident radiation. $S(E)$ is normalized to unity. Its value in the wings of the phonon spectrum is estimated by $\overline{S} \approx (1 - f)/2k_BT$, where f is the recoilless fraction and k_BT is the thermal energy. In the present experiment, typical values were $f = 0.8$, $k_BT = 25$ meV, $\rho\sigma = 10^3$, $\Gamma\overline{S} = 2 \times 10^{-8}$, and $I_0 = 10^8$ Hz. The estimated flux of delayed fluorescence photons is then $\overline{I} = 10^3$ Hz. Further corrections for absorption in the sample, detector efficiency, and coverage of solid angle finally lead to the observed counting rates of ~20 Hz.

In extracting $S(E)$ from the measured data, one faces the problem of determining ρ for each sample. Difficulties occur because of the sharp increase in attenuation of the incident synchrotron radiation at the nuclear resonance. To illustrate the situation, we give the electronic and nuclear contributions to the attenuation length in the case of iron metal. The nuclear part is 0.09 μm at the elastic peak and takes an average value of 0.36 m in the wings of the spectra. The electronic part is constantly 20 μm. Therefore, for thick samples as in the present experiment, the effective number of nuclei that participate in the scattering is strongly decreased at the nuclear resonance and the elastic peak in the data is reduced in height by an essentially unknown factor. This normalization problem is solved by using the general property of $S(E)$ that its first moment equals the recoil energy $E_R = (\hbar^2 k^2)/2M$ (1.94 meV for ^{57}Fe) of the nucleus [19]. This relation permits a calculation of the integrated inelastic spectrum A from the measured spectrum $I_m(E)$,

$$A = \frac{1}{E_R} \int I_m(E) E \, dE - \frac{1}{E_R} \int R(E) E \, dE \int I_m(E) \, dE \,. \tag{3}$$

The second term in this expression accounts for the slight correction that is necessary if the measured intensity $I_m(E)$, instead of $I(E)$ as given by Eq. (1), is used to calculate the first moment. The resolution function $R(E)$ gives the energy distribution of the incident synchrotron radiation and it is usually very close to being symmetric. Therefore, the correction term becomes very small. The phonon spectra are now easily normalized without complicated calculations of ρ that would involve sample geometry and composition. The pure phonon excitation spectrum results after the central peak is removed by fitting and subtraction. The normalized spectra of α-iron and stainless steel after removal of the central peak are shown in Fig. 1. The integrated spectra directly give the recoilless fraction or Lamb-Mössbauer factor

$$f = 1 - \frac{1}{A} \int I'_m(E) \, dE \,, \tag{4}$$

where $I'_m(E)$ denotes the phonon spectrum after removal of the central peak. In contrast to Mössbauer transmission spectroscopy [20] and synchrotron radiation Mössbauer spectroscopy [11,21], Eq. (4) does not require specific knowledge about isotopic abundance, shape or thickness of the sample, resonant cross section, or hyperfine interactions. The Lamb-Mössbauer factor of α-iron was determined to be $f = 0.805(3)$. From the phonon DOS, as shown in Fig. 2, we calculated the recoilless fraction at zero temperature to be $f_0 = 0.9241(7)$ and a ratio of $f/f_0 = 0.871(4)$. This is in agreement with earlier results of $f/f_0 = 0.866(3)$ [11].

For further processing of the data, we assumed the sample material to behave like a harmonic lattice with well-defined phonon states. An expansion of $S(E)$ in terms of n phonon contributions is then straightforward [22]

$$\begin{aligned} S(E) &= f\delta(0) + f \sum_{n=1}^{\infty} S_n(E) \,, \\ S_1(E) &= \frac{E_R \mathcal{D}(E)}{E(1 - e^{-\beta E})} \,, \\ S_n(E) &= \frac{1}{n} \int S_{n-1}(E - \epsilon) S_1(\epsilon) \, d\epsilon, \qquad n \geq 2 \,. \end{aligned} \tag{5}$$

The phonon DOS $\mathcal{D}(E)$ is proportional to the one-phonon term in this expansion. Generally the ratio of the n- and $(n - 1)$-phonon terms is given by $-(\ln f)/n$, which results in a multiphonon contribution of less than 15% for the present data. We deconvoluted the measured

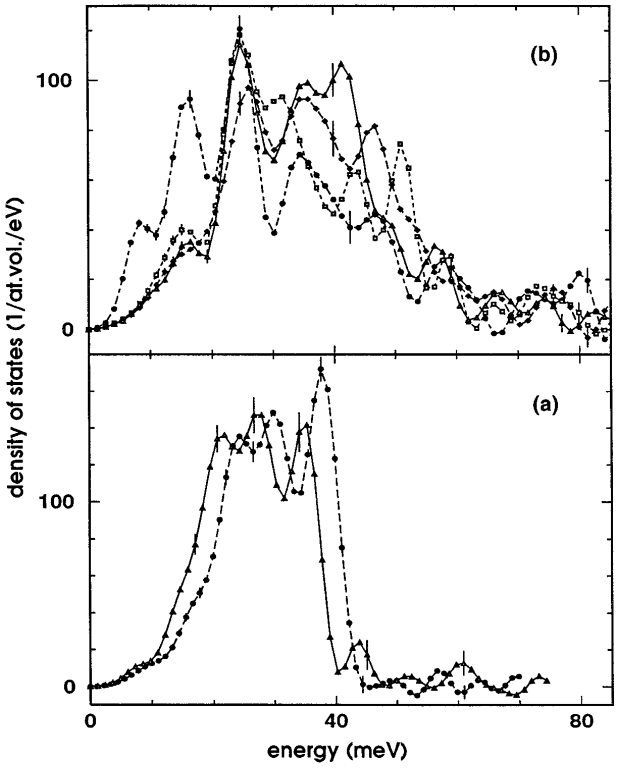

FIG. 2. The phonon DOS of different materials are shown. (a) α-iron (circles, dashed line) and stainless steel (triangles, solid line). (b) $SrFeO_x$ with $x = 3$ (triangles, solid line), $x = 2.86$ (diamonds, dashed line), $x = 2.74$ (rectangles, dotted line), and $x = 2.5$ (circles, dashed-dotted line).

spectra with the resolution function that was fitted to the central peak and applied Eq. (5) to recover the phonon DOS. The results are shown in Fig. 2. In the case of α-iron, $\mathcal{D}(E)$ shows several critical points as predicted [2], although the features are smeared out, most likely due to phonon lifetime effects. The structures above 45 meV are residuals that arise from the deconvolution procedure. If the energy scale of the phonon DOS of stainless steel is stretched by 8%, then the acoustic modes exhibit strong similarities with those of α-iron. This indicates a reduced coupling of about 16%, which might be related to the change in local symmetry from bcc for α-iron to fcc for stainless steel. Dramatic differences occur in the phonon DOS of $SrFeO_x$ while the system undergoes structural changes from cubic perovskite for $x = 3.0$ to tetragonal perovskite with vacancy ordering for $x = 2.86$ to orthohombic perovskite with vacancy ordering for $x = 2.74$ and finally to brownmillerritelike orthorhombic for $x = 2.5$ [23]. Most striking are the persistent phonon modes at 25 meV and the increase of soft-phonon modes at 8 and 16 meV for the brownmilleritelike structure.

From the phonon DOS, we derived the vibrational contribution to the specific heat at constant volume. For α-iron, we determine a value of 23.8(3) J/K mol. The difference between this value and the thermometrically determined value 25.1 J/K mol [24] is attributed to the electronic contribution to the specific heat. It was measured as 1.5 J/K mol [25], which is in agreement with the present evaluation.

In conclusion, we presented measurements of phonon DOS by inelastic nuclear resonant scattering of synchrotron radiation for a number of compounds. This technique allows direct determination of phonon DOS for small samples ($\approx$3 mg in the present experiment) with excellent signal-to-noise ratio ($S/N \approx 10^3$) in a very short time (several minutes at third-generation synchrotron radiation sources). The energy resolution is variable and can be reduced to $\sim$1 meV using crystal optics or even to μeV levels via nuclear resonant filtering of the incident synchrotron radiation. The information that can be derived from such measurements can be used to support existing or develop new models for the interatomic forces and for the coupling of phonons to other quasiparticles. Thus, for example, vibrational entropies and other thermodynamical properties of order-disorder alloys can be studied and temperature-dependent phonon spectra can provide data about the phonon interaction. In addition, materials with noncrystalline structure, such as glasses and liquids, can easily be investigated on the basis of a trend analysis.

The authors acknowledge the support of the TRISTAN accelerator group at KEK. The work at Argonne is supported by the U.S. Department of Energy BES-Materials Science under Contract No. W-31-109-ENG-38. The work at NIU is supported by NSE (Contract No. DMR 93-10656) and the State of Illinois under HECA.

[1] B. N. Brockhouse, in *Inelastic Scattering of Neutrons in Solids and Liquids* (International Atomic Energy Agency, Vienna, 1961).
[2] V. J. Minkievicz, G. Shirane, and R. Nathans, Phys. Rev. **162**, 528 (1967).
[3] B. N. Brockhouse, H. Abou-Helal, and E. D.. Hallmann, Solid State Commun. **5**, 211 (1967).
[4] G. Gilat and L. J. Raubenheimer, Phys. Rev. **144**, 390 (1965).
[5] E. Burkel, *Inelastic Scattering of x-Rays with Very High Energy Resolution* (Springer-Verlag, New York, 1991).
[6] M. Seto, Y. Yoda, S. Kikuta, X. W. Zhang, and M. Ando, preceding Letter, Phys. Rev. Lett. **74**, xxxx (1995).
[7] E. Gerdau, R. Rüffer, H. Winkler, W. Tolksdorf, C. P. Klages, and J. P. Hannon, Phys. Rev. Lett. **54**, 835 (1985).
[8] W. Sturhahn, E. Gerdau, R. Hollatz, R. Rüffer, H. D. Rüter, and W. Tolksdorf, Europhys. Lett. **14**, 821 (1991).
[9] E. E. Alp, T. M. Mooney, T. S. Toellner, W. Sturhahn, E. Witthoff, R. Röhlsberger, E. Gerdau, H. Homma, and M. Kentjana, Phys. Rev. Lett. **70**, 3351 (1993).
[10] W. Sturhahn and E. Gerdau, Phys. Rev. B **49**, 9285 (1994).
[11] U. Bergmann, S. D. Shastri, D. P. Siddons, B. W. Batterman, and J. B. Hastings, Phys. Rev. B **50**, 5957 (1994).
[12] R. L. Cohen, G. L. Miller, and K. W. West, Phys. Rev. Lett. **41**, 381 (1978).
[13] U. Bergmann, J. B. Hastings, and D. P. Siddons, Phys. Rev. B **49**, 1513 (1994).
[14] L. Van Hove, Phys. Rev. **95**, 249 (1954).
[15] K. S. Singwi and A. Sjölander, Phys. Rev. **120**, 1093 (1960).
[16] X. Zhang, T. Mochizuki, H. Sugiyama, S. Yamamoto, H. Kitamura, T. Sioya, M. Ando, Y. Yoda, T. Ishikawa, S. Kikuta, and C. K. Suzuki, Rev. Sci. Instrum. **63**, 404 (1992).
[17] T. M. Mooney, T. S. Toellner, W. Sturhahn, E. E. Alp, and S. D. Shastri, Nucl. Instrum. Methods Phys. Res., Sect. A **347**, 348 (1994).
[18] T. S. Toellner, W. Sturhahn, E. E. Alp, P. A. Montano, and M. Ramanathan, Nucl. Instrum. Methods Phys. Res., Sect. A **350**, 595 (1994).
[19] H. J. Lipkin, Ann. Phys. (Paris) **9**, 332 (1960).
[20] B. R. Bullard, J. G. Mullen, and G. Schupp, Phys. Rev. B **43**, 7405 (1991).
[21] E. E. Alp, W. Sturhahn, and T. S. Toellner, Nucl. Instrum. Mehods Phys. Res., Sect. B (to be published).
[22] W. Marshall and S. W. Lovesey, *Theory of Thermal Neutron Scattering* (Oxford University Press, London, 1971).
[23] Y. Takeda, K. Kanno, T. Takada, O. Yamamoto, M. Takano, N. Nakayama, and Y. Bando, J. Solid State Chem. **63**, 237 (1986).
[24] L. S. Darken and R. P. Smith, Ind. Eng. Chem. **43**, 1815 (1951).
[25] N. W. Ashcroft and N. D. Mermin, *Solid State Physics* (W. B. Saunders Company, Philadelphia, 1976).

NOTES

NOTES